Importance of Local Pattern Properties in Spiral Defect Chaos

David A. Egolf,* Ilarion V. Melnikov, and Eberhard Bodenschatz
Laboratory of Atomic and Solid State Physics, Cornell University, Ithaca, New York 14853-2501
(Received 16 October 1997)

We analyze experimental data from Rayleigh-Bénard convection in a large aspect ratio cell using a new, efficient method applicable to disordered striped patterns from biological, chemical, optical, and fluid systems. We present statistics of various local pattern properties such as the local wave-vector magnitude, local pattern orientation, and defect densities. Using these statistics, we provide quantitative evidence demonstrating that the stability boundaries derived for infinite systems are applicable to local patches within disordered patterns. We also present the first experimental observation of multiple length scales within spiral defect chaos. [S0031-9007(98)05734-2]

PACS numbers: 05.45.+b, 47.20.Lz, 47.52.+j, 47.54.+r

From the ripples in windblown sand to the coats of zebras, the natural world abounds with locally striped patterns. Such patterns have been of great interest throughout history, and, in the last twenty years, scientists in a wide variety of fields have been studying the patterns formed in well-controlled experiments that yield enormous quantities of high-precision data [1]. Experiments involving phenomena as diverse as chemical reactions in shallow layers [2], ferromagnetic films [3], periodically shaken layers of sand [4], excitations in the visual cortex [5], ferrofluids confined between glass plates [6], and block copolymer films [7] often display locally striped patterns. For large aspect ratio systems (many stripes), the patterns are often spatially and temporally disordered but are still locally striped as seen, for example, in Fig. 1(a). Fast, quantitative methods are needed to characterize the complex patterns as a function of experimental parameters, as well as the dynamical behavior of patterns for fixed experimental parameters.

In this Letter we present an efficient, quantitative real-time method for calculating local pattern properties, and we use these properties to analyze spatiotemporal chaotic data from experimental Rayleigh-Bénard convection. By computing the local wave-vector field, we provide experimental evidence that stability boundaries determined for infinite systems may apply *locally* within disordered patterns. Our data also demonstrate the presence of multiple length scales within the spiral defect chaos state of Rayleigh-Bénard convection, perhaps providing a separation of short-scale highly chaotic dynamics and longer-scale phase behavior.

Local pattern properties.—The use of local pattern properties to describe patterns similar to Fig. 1(a) was previously explored by several researchers. As early as 1983, Ahlers *et al.* measured local wave numbers in Taylor vortex flow to understand wave number readjustment in response to changes in system parameters [8]. A few years later, Heutmaker and Gollub [9] performed a detailed study of the wave-vector field and statistics such as "roll bending" and "roll obliqueness" in stationary and time-dependent patterns in circular Rayleigh-Bénard convection cells to understand the stability of convective

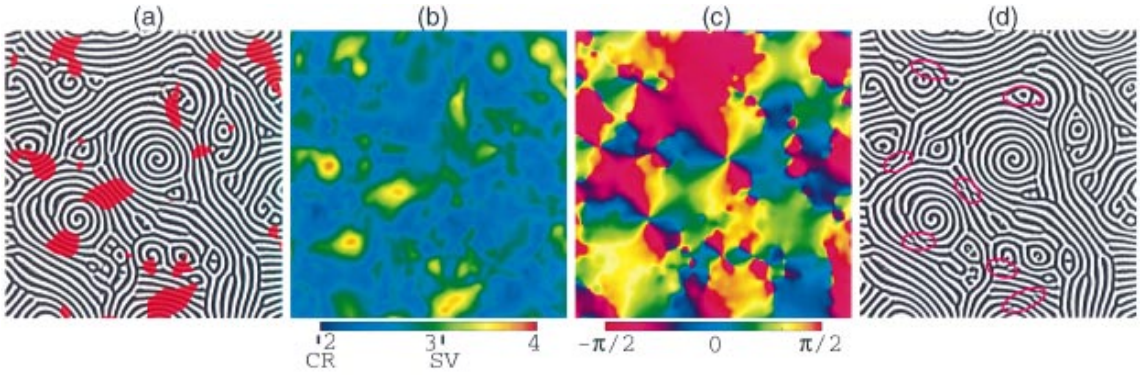

FIG. 1(color). (a) Shadowgraph image of Rayleigh-Bénard convection with Prandtl number $\sigma = 1$ and reduced Rayleigh number $\epsilon = 0.805$. The experimental cell is square of size $\Gamma = L/d = 100$, where d is the depth of the cell and L is the lateral extent. White indicates cold downflow, while black signals warm upflow. Red denotes regions for which the local wave number $|\vec{k}(\vec{x})|$ exceeds the skewed-varicose instability line. (b) Local wave-director magnitude $|\vec{k}(\vec{x})|$ and (c) local roll orientation $\theta(\vec{x})$ for the pattern shown in (a). (d) Shadowgraph image 10 s ($\approx 4\tau_T$, where the vertical thermal diffusion time scale $\tau_T = d^2/\kappa$ and κ is the thermal diffusivity) after image shown in (a). (Figure shows only central $88d \times 90d$ of cell.)

 0031-9007/98/80(15)/3228(4)$15.00

patterns. More recently, Hu *et al.* [10] proposed an order parameter based on measurements of local wave numbers and curvatures for experimental pictures very similar to Fig. 1(a). In a numerical study of a model of Rayleigh-Bénard convection rotated about a vertical axis, Cross *et al.* [11] computed local roll orientations to characterize domain structure. Ouyang and Swinney [2] used the local orientation to analyze patterns in a chemical reaction-diffusion system, and Gunaratne *et al.* [12] suggested an invariant measure of disorder in locally striped patterns. In a set of recent papers, Newell and co-workers [13] have begun to use local wave numbers to study the behavior of phase-diffusion equations in the presence of defects.

These studies clearly demonstrated the potential utility of local pattern properties. Researchers used a variety of methods including nonlinear least squares fits to small patches of patterns [12], automated [10] and semi-automated [9] determination of pattern "skeletons," modern wavelet-based procedures for determination of wave-vector fields [2,11,13], and visual identification of spirals [14]. In this Letter we present a simple algorithm for the real-time quantitative analysis of patterns found in today's large aspect ratio experiments, thus opening new avenues of research on these systems.

A new method.—For patterns that are locally striped, we can approximate the field $u(\vec{x})$ locally by

$$u(\vec{x}) = A(\vec{x}) \cos[\phi(\vec{x})], \tag{1}$$

for which the local wave vector $\vec{k}(\vec{x})$ is defined via

$$\vec{k}(\vec{x}) \equiv \vec{\nabla}\phi(\vec{x}). \tag{2}$$

Sufficiently far from defects, we expect that variations in $A(\vec{x})$ and $\vec{k}(\vec{x})$ are small compared to variations in $\phi(\vec{x})$. The components of the wave vector $\vec{k}(\vec{x})$ can then be approximated well using simple partial derivatives. Specifically,

$$|k_x|^2 = -\frac{\partial_x^2 u(\vec{x})}{u(\vec{x})}, \tag{3}$$

where $k_x = \vec{k} \cdot \hat{x}$ and $\partial_x^2 \equiv \partial^2/\partial x^2$.

Equation (3) and the analogous equation for $|k_y|^2$ yield only the *magnitudes* of the wave-vector components k_x and k_y. From these magnitudes, the vector can be specified in any of four directions. We note, however, that in a real field the wave vector (k_x, k_y) is equivalent to $(-k_x, -k_y)$; i.e., $\vec{k}(\vec{x})$ is actually a *director* field $\overleftrightarrow{k}(\vec{x})$, so we only need to determine the sign of k_y relative to k_x. We find this using a mixed partial derivative. If we choose $k_x > 0$,

$$k_y = -|k_y| \operatorname{sgn}\left(\frac{\partial_{xy} u(\vec{x})}{u(\vec{x})}\right), \tag{4}$$

where $\operatorname{sgn}(v) = v/|v|$ and $|k_y|$ is determined using the equation analogous to Eq. (3).

Because this method is local, the effects of noise, of higher harmonics, and of amplitude and wave-vector variations neglected in Eq. (1) are often noticeable. We reduce these effects by smoothing the director field $\overleftrightarrow{k}(\vec{x})$ over small regions. The k_x and k_y fields are first screened for anomalous values due to defects or due to the denomimator $u(\vec{x})$ in Eq. (3) approaching very close to zero. (The radius of strong amplitude and wave-vector variations around a defect is about $\lambda/2$, where λ is approximately the average wavelength in the pattern.) The few anomalous values are replaced by neighboring values. The director field $\overleftrightarrow{k}(\vec{x}) = k_x + ik_y$ is then smoothed in two parts—$k^2(\vec{x}) = k_x^2(\vec{x}) + k_y^2(\vec{x})$ and $\exp[i2\theta(\vec{x})]$, where $\theta(\vec{x})$ is defined implicitly through the relation $\exp[i\theta(\vec{x})] = \overleftrightarrow{k}(\vec{x})/|\overleftrightarrow{k}(\vec{x})|$. Each smoothing is accomplished using a simple Gaussian blur of radius $\lambda/2$. This particular choice of the smoothing radius removes most of the contributions from higher harmonics and amplitude variations without obscuring variations on length scales larger than the order of a wavelength [15].

We have carefully tested our method on a variety of computer generated patterns, as well as on simulations of straight rolls in Rayleigh-Bénard convection, for which the root-mean-square deviation of the calculated local wave number from the known value was found to be 0.7%. For straight rolls filling an experimental Rayleigh-Bénard convection cell, the error in the local wave number was less than the uncertainties in the experimentally determined value from the power spectrum. For a pattern of 512×512 pixels, the entire procedure, including the calculation of the raw director field and the smoothing of the field, takes about 1 s on a modern workstation. Although in this Letter we present only patterns from experimental Rayleigh-Bénard convection, we have successfully applied our method to patterns from a variety of other systems, including vibrating sand layers, block copolymers, magnetic stripe domains, and ferrofluids.

Results.—The pattern (shadowgraph field) in Fig. 1(a) developed in a Rayleigh-Bénard convection experiment in which a horizontal layer of fluid of lateral extent L is confined between two parallel plates with separation d and a temperature difference $\Delta T = T_{\text{bottom}} - T_{\text{top}} > 0$. (For experimental details, see Ref. [16].) For ΔT larger than a critical value ΔT_c, a convective instability develops. In most situations studied experimentally, this instability leads to the development of a striped convective roll pattern with a horizontal wave number $k \approx \pi/d$. For moderate values of the control parameter $\epsilon = (T - T_c)/T_c$ and large system sizes (i.e., many convection rolls), the spatiotemporal chaotic state of spiral defect chaos [shown in Fig. 1(a)] is found.

Figure 1(b) shows the local wave-director magnitude $|\vec{k}(\vec{x})|$ at each point of the experimental data in Fig. 1(a) [17]. The wave number is approximately constant across the pattern as indicated by the large regions of blue-green, but small localized regions of very high (red) wave number are interspersed throughout. These areas correspond to the patches of compressed rolls in Fig. 1(a).

The solid line in Fig. 2 is the distribution of local wave-director magnitudes averaged over a period of 50 h (about 28 horizontal thermal diffusion times). The theoretically determined [18,19] and experimentally confirmed [20] secondary stability boundaries are also shown. A finite region of the distribution is above the upper (skewed-varicose) stability boundary; however, no noticeable amount of the distribution is below the lower (cross-roll) boundary. This is consistent with the observed dynamics showing defects formed through skewed-varicose instabilities and almost no cross-roll events; however, it is in direct contrast to the power spectrum (the circles), which has a finite region extending below the lower boundary. The broadening of the power spectrum (as compared to the local wave-number distribution) is not unexpected since the spectrum contains global modes and needs to describe spatial variations and localized objects such as defects and grain boundaries. However, it has been a common practice to use the power spectrum as an approximation to the local wave-number distribution. Figure 2 demonstrates that the power spectrum should not be used in this manner for disordered patterns such as in Fig. 1(a), since it would incorrectly suggest that the pattern contains regions of rolls with wave numbers below the cross-roll instability.

Even though the stability boundaries shown in Fig. 2 are derived for a system with an infinite number of parallel straight rolls extending to infinity [18], one might hope that the boundaries apply at least approximately to smaller regions of "almost" straight parallel rolls. As mentioned above, we observed in the experimental dynamics numerous skewed-varicose events and almost no cross-roll events. These skewed-varicose events are, in fact, associated with regions in which the local wave number exceeds the skewed-varicose boundary. The red regions in Fig. 1(a) are points with local wave numbers outside the theoretically stable range. Figure 1(d) shows the state of the system 10 s after the state in Fig. 1(a). During that time, several skewed varicose events produced pairs of defects (regions marked by ellipses). Each of these events occurred within the regions of unstable wave number in Fig. 1(a). This evidence suggests that even stability analyses performed in the infinite-extent limit may, at least approximately, apply locally.

In addition to the local wave-director magnitude, several other fields can be computed. Figure 1(c) shows the local orientation of the rolls $\theta(\vec{x})$ for the pattern in Fig. 1(a). The winding of the roll orientation about the centers of spirals is particularly clear for the large spiral in the center of the picture. Knowledge of the local orientation of the rolls also allows the identification of disclinations, which can be classified by the number of 2π rotations completed by the director as a defect is circled. Disclinations are easily found by the computer by calculating the winding of $\theta(\vec{x})$ along a closed circuit about the point of interest. Figure 3(b) shows the average number of $\nu = +1$ defects N_d (spirals and targets) as a function of the control parameter ϵ, expressed as a spiral length scale $\xi_d = (A/N_d)^{1/2}$, where A is the area over which spirals and targets are counted.

We have also computed azimuthally averaged autocorrelation functions for the shadowgraph field and the orientation field $\exp[i2\theta(\vec{x})]$. Correlation functions for $\epsilon = 0.805$ are shown in Fig. 3(a); other values of ϵ yield similar plots. For six values of the control parameter ϵ and for both of the correlation functions, we determined correlation lengths ξ from the asymptotic exponential decay of the correlation function, $C(\Delta r) \sim \exp(-\Delta r/\xi)$. As seen in Fig. 3, the correlation lengths corresponding to

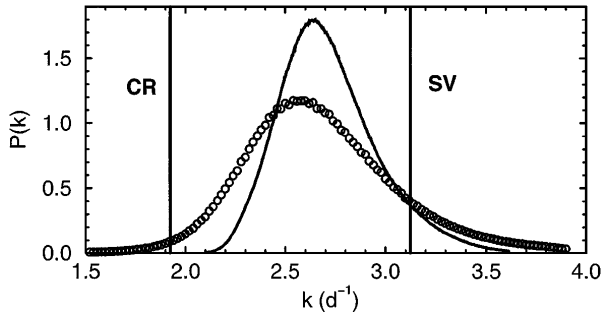

FIG. 2. Probability densities of the local wave number $|\vec{k}(\vec{x})|$ (solid line) and the power spectral density (circles) for $\epsilon = 0.805$ computed from the central $63d \times 62d$ region of 300 images each separated by 10 min ($\approx 240\tau_T$). Vertical lines denote the lower (cross-roll) and upper (skewed-varicose) stability boundaries.

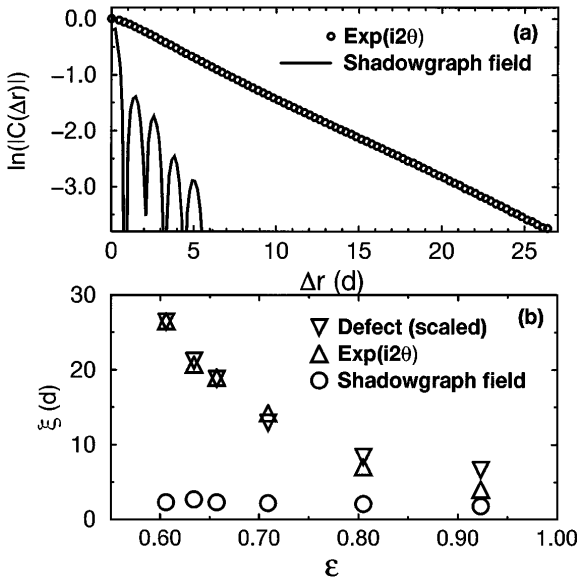

FIG. 3. (a) Azimuthally averaged two-point equal-time correlation functions of the orientation field $\exp(i2\theta)$ and the high-pass-filtered shadowgraph field. (b) Correlation lengths of the orientation field and of the shadowgraph field. Also plotted is the scaled spiral length scale $\xi_d/3.5$. Experimental details can be found in Ref. [16].

the orientation grow quite large as ϵ is decreased. These data signal that at least two independent length scales are present since the correlation length of the shadowgraph field itself are quite short and only change slightly over the same range of ϵ [16,21,22]. The new longer length scale seems to agree well with the size of coherent structures such as spirals within the pattern (and with typical visual estimates of coherence lengths). In particular, the spiral length scale ξ_d coincides with the correlation length of the orientation field to within a factor of order 1. Preliminary evidence from simulations of Rayleigh-Bénard convection suggests that this longer length scale may also be associated with the experimentally unobserved mean flow. In analogy to length scales discovered in other spatiotemporal chaotic states [22–25], we also speculate that the shorter length scale may be associated with the short-range chaotic dynamics.

We have presented a new, efficient method that allows real-time analysis of the local pattern properties of data gathered in modern large aspect ratio pattern-forming experiments involving biological, chemical, optical, and fluid systems. We have provided quantitative experimental evidence that the secondary stability boundaries are valid locally, and we have demonstrated the existence of at least two length scales within the spatiotemporal chaotic state of spiral defect chaos.

We are grateful to W. Pesch for many stimulating discussions and for the use of his code for simulating the Boussinesq equations. We also thank G. Ahlers, R. Cakmur, R. Ecke, H. Greenside, S. Morris, B. Plapp, H. Riecke, and J. Socolar for useful discussions. This work was supported by the National Science Foundation (ASC-9503963, DMR-9320124, DMR-9705410, and DMR-9419506), by NATO (CRG-950243), and by the Cornell Theory Center.

*Electronic address: egolf@tc.cornell.edu

[1] M. C. Cross and P. C. Hohenberg, Rev. Mod. Phys. **65**, 851 (1993).
[2] Q. Ouyang and H. L. Swinney, Chaos **1**, 411 (1991).
[3] M. Seul and R. Wolfe, Phys. Rev. Lett. **68**, 2460 (1992).
[4] F. Melo, P. Umbanhower, and H. L. Swinney, Phys. Rev. Lett. **75**, 3838 (1995).
[5] W. M. Kistler, R. Seitz, and J. L. van Hemmen (to be published).
[6] R. E. Rosensweig, Sci. Am. **247**, No. 4, 137 (1982).
[7] Figure 6 in T. A. Witten, Phys. Today **43**, No. 7, 21 (1990).
[8] G. Ahlers, D. S. Cannell, and M. A. Dominguez Lerma, Phys. Rev. A **27**, 1225 (1983).
[9] M. S. Heutmaker and J. P. Gollub, Phys. Rev. A **35**, 242 (1987).
[10] Y. Hu, R. E. Ecke, and G. Ahlers, Phys. Rev. E **51**, 3263 (1995); Phys. Rev. Lett. **74**, 391 (1995); Y. Hu, Ph.D. thesis, University of California, Santa Barbara, 1995 (unpublished).
[11] M. C. Cross, D. Meiron, and Y. Tu, Chaos **4**, 607 (1994).
[12] G. H. Gunaratne, R. Jones, Q. Ouyang, and H. L. Swinney, Phys. Rev. Lett. **75**, 3281 (1995).
[13] See, e.g., A. C. Newell *et al.*, Physica (Amsterdam) **97D**, 185 (1996); C. Bowman and A. C. Newell, Rev. Mod. Phys. **70**, 289 (1998).
[14] R. E. Ecke, Y. Hu, R. Mainieri, and G. Ahlers, Science **269**, 1704 (1995).
[15] The size of the smoothing region is easily determined empirically since local higher harmonics will appear as obvious modulations to the wave-number field.
[16] R. V. Cakmur, D. A. Egolf, B. B. Plapp, and E. Bodenschatz, Phys. Rev. Lett. **79**, 1853 (1997).
[17] Experimental data were prefiltered to remove noise, higher harmonics, and long wavelength variations of the mean. Low-pass and high-pass hyperbolic tangent Fourier filters of width $0.1d^{-1}$ were applied to the raw shadowgraph data. The low-pass filter was centered at $k = 1.0d^{-1}$ to remove long wavelength variations of the mean. The high-pass filter was centered at the lowest point of the power spectrum between the primary and second harmonics. The results are not sensitive to small changes in wave-number cutoffs or the tangent widths.
[18] R. M. Clever and F. H. Busse, J. Fluid Mech. **65**, 625 (1974).
[19] W. Pesch (private communication).
[20] See, e.g., V. Croquette, Contemp. Phys. **30**, 113 (1989), and references therein.
[21] S. W. Morris, E. Bodenschatz, D. S. Cannell, and G. Ahlers, Phys. Rev. Lett. **71**, 2026 (1993).
[22] S. W. Morris, E. Bodenschatz, D. S. Cannell, and G. Ahlers, Physica (Amsterdam) **97D**, 164 (1996).
[23] D. A. Egolf and H. S. Greenside, Nature (London) **369**, 129 (1994).
[24] D. A. Egolf and H. S. Greenside, Phys. Rev. Lett. **74**, 1751 (1995).
[25] C. S. O'Hern, D. A. Egolf, and H. S. Greenside, Phys. Rev. E **53**, 3374 (1996).